



**NAVAL
POSTGRADUATE
SCHOOL**

MONTEREY, CALIFORNIA

THESIS

**AEROSOL OPTICAL DEPTH MODEL ASSESSMENT
WITH HIGH RESOLUTION MULTIPLE ANGLE SENSORS**

by

Joseph S. Martin

December 2004

Thesis Advisor:
Second Reader:

Philip A. Durkee
Kurt E. Nielsen

Approved for public release; distribution is unlimited

THIS PAGE INTENTIONALLY LEFT BLANK

REPORT DOCUMENTATION PAGE

Form Approved OMB No. 0704-0188

Public reporting burden for this collection of information is estimated to average 1 hour per response, including the time for reviewing instruction, searching existing data sources, gathering and maintaining the data needed, and completing and reviewing the collection of information. Send comments regarding this burden estimate or any other aspect of this collection of information, including suggestions for reducing this burden, to Washington headquarters Services, Directorate for Information Operations and Reports, 1215 Jefferson Davis Highway, Suite 1204, Arlington, VA 22202-4302, and to the Office of Management and Budget, Paperwork Reduction Project (0704-0188) Washington DC 20503.

1. AGENCY USE ONLY (Leave blank)	2. REPORT DATE December 2004	3. REPORT TYPE AND DATES COVERED Master's Thesis
4. TITLE AND SUBTITLE: Aerosol Optical Depth Model Assessment With High Resolution Multiple Angle Sensors		5. FUNDING NUMBERS
6. AUTHOR(S) Joseph S. Martin		8. PERFORMING ORGANIZATION REPORT NUMBER
7. PERFORMING ORGANIZATION NAME(S) AND ADDRESS(ES) Naval Postgraduate School Monterey, CA 93943-5000		
9. SPONSORING /MONITORING AGENCY NAME(S) AND ADDRESS(ES) N/A		10. SPONSORING/MONITORING AGENCY REPORT NUMBER
11. SUPPLEMENTARY NOTES The views expressed in this thesis are those of the author and do not reflect the official policy or position of the Department of Defense or the U.S. Government.		
12a. DISTRIBUTION / AVAILABILITY STATEMENT Approved for public release; distribution is unlimited		12b. DISTRIBUTION CODE

13. ABSTRACT (maximum 200 words)

This thesis assesses the performance of the Naval Postgraduate School Aerosol Optical Depth (NPS AOD) model utilizing very high spatial resolution QuickBird (QB) satellite data. QuickBird derived AOD results are compared to other satellite and ground based AOD results, specifically, AErosol RObotic NETwork (AERONET), MODerate resolution Imaging Spectroradiometer (MODIS), Multi-angle Imaging SpectroRadiometer (MISR), and Advanced Very High Resolution Radiometer (AVHRR). Data is collected around Sir Bu Nuair Island, United Arab Emirates in September 2004 as part of the UAE² Campaign. Satellite measured radiances are calibrated and due to spatial resolution differences between sensors, modal radiances are calculated for areas matching the highest resolution sensor. The AOD model is based on AVHRR wavelengths; hence, the modal satellite measured radiances are linearly extrapolated to the effective wavelengths of AVHRR. Results show application of the NPS AOD model to QuickBird data yields findings that are consistent with other satellite and ground based retrievals. In general, the NPS AOD model works well for nadir and near-nadir view angles, but not for high zenith angles.

14. SUBJECT TERMS Aerosol Optical Depth, AOD, MISR, MODIS, QuickBird, AERONET, AVHRR		15. NUMBER OF PAGES 53
16. PRICE CODE		
17. SECURITY CLASSIFICATION OF REPORT Unclassified	18. SECURITY CLASSIFICATION OF THIS PAGE Unclassified	19. SECURITY CLASSIFICATION OF ABSTRACT Unclassified
		20. LIMITATION OF ABSTRACT UL

THIS PAGE INTENTIONALLY LEFT BLANK

Approved for public release; distribution is unlimited

**AEROSOL OPTICAL DEPTH MODEL ASSESSMENT WITH HIGH
RESOLUTION MULTIPLE ANGLE SENSORS**

Joseph S. Martin
Lieutenant Commander, United States Navy
B.S., University of Washington, 1992

Submitted in partial fulfillment of the
requirements for the degree of

**MASTER OF SCIENCE IN METEOROLOGY AND PHYSICAL
OCEANOGRAPHY**

from the

NAVAL POSTGRADUATE SCHOOL
December 2004

Author: Joseph S. Martin

Approved by: Philip A. Durkee
Thesis Advisor

Kurt E. Nielsen
Second Reader

Philip A. Durkee
Chairman, Department of Meteorology

THIS PAGE INTENTIONALLY LEFT BLANK

ABSTRACT

This thesis assesses the performance of the Naval Postgraduate School Aerosol Optical Depth (NPS AOD) model utilizing very high spatial resolution QuickBird (QB) satellite data. QuickBird derived AOD results are compared to other satellite and ground based AOD results, specifically, AErosol RObotic NETwork (AERONET), MODerate resolution Imaging Spectroradiometer (MODIS), Multi-angle Imaging SpectroRadiometer (MISR), and Advanced Very High Resolution Radiometer (AVHRR). Data is collected around Sir Bu Nuair Island, United Arab Emirates in September 2004 as part of the UAE² Campaign. Satellite measured radiances are calibrated and due to spatial resolution differences between sensors, modal radiances are calculated for areas matching the highest resolution sensor. The AOD model is based on AVHRR wavelengths; hence, the modal satellite measured radiances are linearly extrapolated to the effective wavelengths of AVHRR. Results show application of the NPS AOD model to QuickBird data yields findings that are consistent with other satellite and ground based retrievals. In general, the NPS AOD model works well for nadir and near-nadir view angles, but not for high zenith angles.

THIS PAGE INTENTIONALLY LEFT BLANK

TABLE OF CONTENTS

I.	INTRODUCTION.....	1
II.	BACKGROUND	3
	A. RADIATIVE TRANSFER THEORY.....	3
	B. OPTICAL DEPTH.....	4
	C. PREVIOUS APPROACHES	5
III.	DATA	7
	A. GENERAL DATA DESCRIPTION.....	7
	B. INSTRUMENTS	7
	1. QuickBird (QB).....	7
	2. Multi-angle Imaging SpectroRadiometer (MISR).....	8
	3. MODerate Resolution Imaging Spectroradiometer (MODIS)	11
	4. Advanced Very High Resolution Radiometer (AVHRR).....	11
	5. AErosol RObotic NETwork (AERONET).....	12
IV.	METHODS AND PROCEDURES.....	15
	A. AERONET DATA	15
	B. SATELLITE DATA.....	15
	C. AOD ALGORITHMS.....	20
	1. NPS	20
	2. MISR	22
	3. NPS vs. MISR	23
V.	RESULTS	25
	A. SYNOPTIC WEATHER SITUATION.....	25
	B. AOD COMPARISONS.....	27
VI.	CONCLUSIONS AND RECOMMENDATIONS.....	33
	A. CONCLUSIONS	33
	B. RECOMMENDATIONS.....	34
	LIST OF REFERENCES.....	35
	INITIAL DISTRIBUTION LIST	37

THIS PAGE INTENTIONALLY LEFT BLANK

LIST OF FIGURES

Figure 1.	Overview of QB scenes at 60, 37, and 61-degree view angles, respectively © 2004 DigitalGlobe, Inc. All rights reserved).....	8
Figure 2.	Red wavelength of AVHRR, MODIS, MISR, MODIS and QB and increasing spatial resolutions © 2004 DigitalGlobe, Inc. All rights reserved).....	16
Figure 3.	MISR full-scene red and NIR band histograms.....	17
Figure 4.	MISR true color image indicating areas of significant red modal radiance peaks	17
Figure 5.	QuickBird nadir view red and NIR band histograms with annotated observed radiances.....	18
Figure 6.	Wehrli solar irradiance spectrum with applicable satellite bandwidths.....	19
Figure 7.	Red modal top of the atmosphere radiance (L_t) vs. scattering angle	20
Figure 8.	Transmittance as a function of wavelength with applicable sensor bandwidths and atmospheric absorption gases.....	21
Figure 9.	Scatter plot with satellite derived AOD's and surface based AOD's (From Smith 1998).....	22
Figure 10.	Left image of SBN is a true color nadir QuickBird view; Right image of SBN applies a histogram equalization enhancement to the left image © 2004 DigitalGlobe, Inc. All rights reserved).....	26
Figure 11.	Abu Dhabi, UAE 00Z 19 Sep 2004 sounding indicating an inversion near 925 mb or 700 m (From University of Wyoming 2004).	27
Figure 12.	AERONET estimated AOD values at seven wavelengths from 0500- 0900Z. Vertical lines, from left to right, indicate satellite overpass times for QB, MODIS, MISR, and AVHRR, respectively.....	29
Figure 13.	NPS AOD63 (red band) calculated values versus satellite zenith angle. The dashed line indicates the MISR AOD value and the box shows the SBN AERONET estimated AOD range.....	30
Figure 14.	S12 Size Index versus Satellite Scattering Angle with Brown (1997) Aerosol Model Size Distributions.....	31
Figure 15.	Angstrom Exponent estimated by AERONET between 0500-0900Z	31

THIS PAGE INTENTIONALLY LEFT BLANK

LIST OF TABLES

Table 1.	QB bandwidth and spatial resolutions (After DigitalGlobe 2004)	8
Table 2.	MISR telescope angles and spatial resolutions (From JPL 2004)	10
Table 3.	MISR bands primary and secondary uses (From JPL 2004)	10
Table 4.	MODIS bands used in study: primary uses, resolutions, and bandwidths (After GSFC 2004)	11
Table 5.	AVHRR bands used in study: spectral and spatial resolution (After NOAA KLM Users Guide 2004)	12
Table 6.	Scattering angle, view angle, S12 ratio, aod63, aod86, 660-840 Angstrom Exponent sorted by sensor. Green shaded blocks are within 11% of SBN (shaded blue). The SBN estimated Angstrom Exponent is at 500-870 nm. ...	28

THIS PAGE INTENTIONALLY LEFT BLANK

ACKNOWLEDGMENTS

I would like to thank my advisor, Dr. Philip A. Durkee of the Department of Meteorology, Naval Postgraduate School, for his guidance, support, and understanding during the thesis process.

A huge thanks to Mr. Kurt Nielsen for his technical expertise, personal support, ideas, and tremendous data processing efforts through the thesis process. Without Kurt, I would still be trying to get data.

I would like to thank LCDR Jake Hinz, LCDR Nick Vincent, LT John Marburger, LT Billy Roeting, and LT Roland Clark for their camaraderie and support during our time at NPS. A special thanks to LCDR Nick Vincent for his assistance with the data processing and problem solving.

Additional thanks goes to the scientific teams at NRL Monterey, NASA GSFC, JPL, and DigitalGlobe for their assistance and data contributions used in this study.

Most importantly, I would like to thank my wife, Gwyn. Without her love, support, and patience, none of this would have been possible or at least it would have been much more difficult and less enjoyable.

THIS PAGE INTENTIONALLY LEFT BLANK

I. INTRODUCTION

Knowledge of the distribution of atmospheric aerosols is important in terms of the Earth's radiation budget as well as U.S. Navy and Department of Defense (DOD) electro-optical (EO) weapons systems and sensors. Atmospheric aerosols influence the Earth's radiation budget both directly and indirectly through the modification of cloud properties. The direct effect reflects, scatters, and absorbs some of the incoming solar radiation resulting in reduced heating at the Earth's surface. The indirect effect increases cloud albedo by providing additional condensation nuclei that attract water and form smaller water droplets, increasing the cloud brightness at solar wavelengths and reducing heating at the Earth's surface. This cooling effect offsets anthropogenic greenhouse gas warming by approximately 25 to 50% (IPCC 2001, Twomey *et al.* 1984, Charlson *et al.* 1992, Kiehl and Briegleb 1993).

Atmospheric aerosols influence electro-optical systems performance by the scattering visible and near-infrared (NIR) energy used by these systems. These effects can be especially severe in the near coastal boundaries when EO systems may be subject to marine and continental aerosols. Operators and planners need to be aware of these impacts when planning EO system design and executing missions. Failure to account for aerosol effects on system performance could degrade or prevent mission success. Furthermore, Intelligence, Surveillance, and Reconnaissance (ISR) agencies should be aware of how aerosols may affect their remote sensors in conjunction with Battle Damage Assessment (BDA) and other data gathering activities.

Aerosol characterization information is derivable from *in situ* or remote methods. *In situ* measurements may include ground or air based radiometers, sunphotometers, and spectrometers. This method provides the highest spectral and spatial resolutions and most accurate data, but the data is spatially very sparse. Remote methods rely on satellite-mounted radiometers that, while not as high of resolution as *in situ* measurements, provide better spatial coverage.

Satellite radiometers need to have high radiometric resolution as well as spatial resolution in order to distinguish the minute changes in the red and NIR wavelengths

used for aerosol detection. Recent advances in remote sensing technology have reduced spatial resolutions from 1000m to 3m allowing for high resolution aerosol optical depth (AOD) calculations. This research paper utilizes remotely measured data from DigitalGlobe's QuickBird (QB), National Aeronautics and Space Administration's (NASA) MODerate resolution Imaging Spectroradiometer (MODIS), NASA Multi-angle Imaging SpectroRadiometer (MISR), and National Oceanic and Atmospheric Administration's (NOAA) Advanced Very High Resolution Radiometer (AVHRR), along with *in situ* measured data from an AERONET station in the United Arab Emirates (UAE). AOD calculations using the satellite data rely on earlier work done by Durkee *et al.* (1991), Brown (1997), and Smith (1998). The Naval Postgraduate School (NPS) AOD model utilizes a ratio between the red and NIR channels (Ch 1 and 2) of AVHRR to determine an estimate of the aerosol size distribution that can be used to parameterize the scattering phase function, that is used to calculate the AOD.

The objectives of this study were to assess the performance of the NPS AOD model utilizing very high spatial resolution QuickBird satellite data at varying zenith angles for the first time. QuickBird derived AOD results are compared to other satellite (MODIS, MISR, and AVHRR) and ground based (AERONET) AOD results for the same location and within 30 minutes of each other. Chapter II describes the background and previous AOD retrieval approaches. Chapter III describes the instrumentation used to collect the data. Chapter IV outlines the methodology and procedures used to analyze the data. Chapter V discusses the results of the thesis and Chapter VI provides the conclusions and recommendations for future study.

II. BACKGROUND

A. RADIATIVE TRANSFER THEORY

Radiative transfer theory describes the interaction between atmospheric aerosols and incoming solar irradiance that produces measurable radiance at the top of the atmosphere. The theory states the total diffuse radiation measured at the satellite radiometer is the sum of radiation energy scattered toward the satellite, minus the radiation energy scattered away from the satellite and energy that is absorbed by various gases. Durkee *et al.* (1986) showed the observed radiance at the satellite can be written as:

$$L_t = L_s + L_r + L_a \quad (2.1)$$

where L_s is the radiance leaving the surface, L_r is the radiance due to Rayleigh scattering by air molecules, and L_a is the radiance due to scattering by aerosols. For over water regions, L_s is easily determined due to the low reflectances of water in the red and NIR wavelengths. However, care must be taken to avoid regions of high sun glint that will contaminate L_s by artificially raising measured radiances. Sun glint is avoided through judicious selection of appropriate sun-satellite geometries. L_r can be calculated using a model (e.g. Turner 1973) since atmospheric molecular constituents, such as ozone and water vapor, are nearly uniform in space and time. For over water regions where L_s is small, L_r accounts for most of the energy received at the satellite. Thus, after L_s and L_r have been accounted for, all that remains is L_a . Brown (1997) describes the removal of L_s (including sun glint) and L_r .

The general form of a Radiative Transfer Equation (RTE) (Liou 1980) in a plane parallel atmosphere can be written as:

$$\begin{aligned} \mu \frac{dL_t(0; \mu, \phi)}{d\delta} &= L_t(\delta, \Omega) - \frac{\omega_o}{4\pi} \int L_t(\delta, \Omega') \rho(\Omega, \Omega') d\Omega \\ &\quad - \frac{\omega_o}{4\pi} \pi F_o \rho(\Omega \theta - \Omega_o) e^{-\delta/\mu_o} \end{aligned} \quad (2.2)$$

where μ is the cosine of satellite zenith angle (θ), L_t is the diffuse radiance ($\text{W/m}^2 \mu\text{m sr}$), δ is the optical depth, Ω is the solid angle defined by θ and ϕ , ω_o is the single scatter albedo, p is the scattering phase function, and F_o is the incoming solar radiance at the top of the atmosphere and μ_o is the cosine of solar zenith angle (θ_o).

Durkee *et al.* (1991) found that in a cloudless marine environment, the RTE could be simplified by making the following assumptions: the region is sun glint free, the aerosols are spherical and non-absorbing, and the optical depth is low enough so linear single scattering dominates. Using these assumptions, the solution of the RTE reduces to:

$$L_a = \frac{\omega_o F_o}{4\mu} p(\psi_s) \delta_a \quad (2.3)$$

where the subscript “a” denotes aerosol values. Furthermore, marine aerosols in the visible spectrum are weak absorbers, so ω_o is nearly one. Since F_o is a known constant μ is obtained by the satellite-earth geometry, once the scattering phase function ($p(\psi_s)$) is known, the AOD can be calculated.

B. OPTICAL DEPTH

Brown (1997) and Smith (1998) describe the process to calculate AOD, summarized as follows. Diffuse radiances (L_t) measured at the satellite for the red (AVHRR Ch1) and NIR (AVHRR Ch2) wavelengths have ozone and water vapor corrections applied. A cloud-screening algorithm is applied as is a sun glint check that also considers wind speed. An L_s is assumed based on open ocean chlorophyll concentrations and L_r is calculated according to Turner (1973). The resultant aerosol radiances (L_a) are used to determine the S12 ratio and sun-satellite and earth-satellite geometries are used to calculate the scattering angle. The S12 and scattering angle are used to determine the best aerosol size distribution model to yield the scattering phase function($p(\psi_s)$) used in equation 2.3 to calculate the aerosol optical depth (δ_a).

C. PREVIOUS APPROACHES

Durkee *et al.* (1991) developed the algorithm for AVHRR AOD retrievals and Brown (1997) enhanced the algorithm to include GOES retrievals. Smith (1998) and Kuciauskas (2002) validated the previous work using airborne and ground based sunphotometers and radiometers. This thesis uses the same validated AOD algorithm but applies it to three new sensors: QuickBird, MODIS, and MISR.

THIS PAGE INTENTIONALLY LEFT BLANK

III. DATA

A. GENERAL DATA DESCRIPTION

The data used in this study was collected from polar orbiting satellites over the Arabian Gulf and an AERONET station located on Sir Bu Nuair Island (SBN), UAE (25.217N 054.233E) between 0647 and 0718Z on 19 September 2004. The marine location was chosen to make use of an AERONET station as ground truth and the satellites were chosen based on their nearly coincident overpass times and high spatial resolutions. Data collection and results may also support the United Arab Emirates Unified Aerosol Experiment (UAE²) Campaign (NRL 2004).

B. INSTRUMENTS

1. QuickBird (QB)

The QuickBird instrument is deployed aboard DigitalGlobe's privately owned commercial QUICKBIRD-2 satellite, launched in October 2001. QUICKBIRD-2 is a polar orbiting satellite in a sun-synchronous orbit at an altitude of 450 km with a 98-degree inclination and a period of 93.4 minutes. The sun-synchronous orbit allows QUICKBIRD-2 to pass directly overhead a given location at approximately 1020 local solar time each day and with a 16.5 km swath, provides for global coverage every one to three and a half days (DigitalGlobe 2004).

QUICKBIRD-2 measures solar-reflected energy from sampled areas of the Earth in four spectral bands between 0.450 and 0.900 μm . QUICKBIRD-2 has nominal spatial resolutions 0.6 m for the panchromatic band and 2.44-2.8 m for the multispectral bands. Table 1 lists the bands and maximum spatial resolutions. Figure 1 depicts the three QuickBird scenes imaged for this research paper to test the high zenith angle viewing geometry capabilities of the NPS AOD model. In addition to a nadir collect, forward and aft viewing geometries were collected one minute before and after the nadir collect, respectively. This study uses primarily the red and NIR channels at three view angles; 59.9, 36.9, and 61.2 degrees in the forward, nadir, and aft view directions, respectively. Due to the high view angles used in the study, image pixel size increases from a nominal

2.44 m at nadir (DigitalGlobe 2004) to an effective spatial resolution of approximately 6.8 m, 3.6 m, and 6.9 m for the forward, nadir, and aft views, respectively.

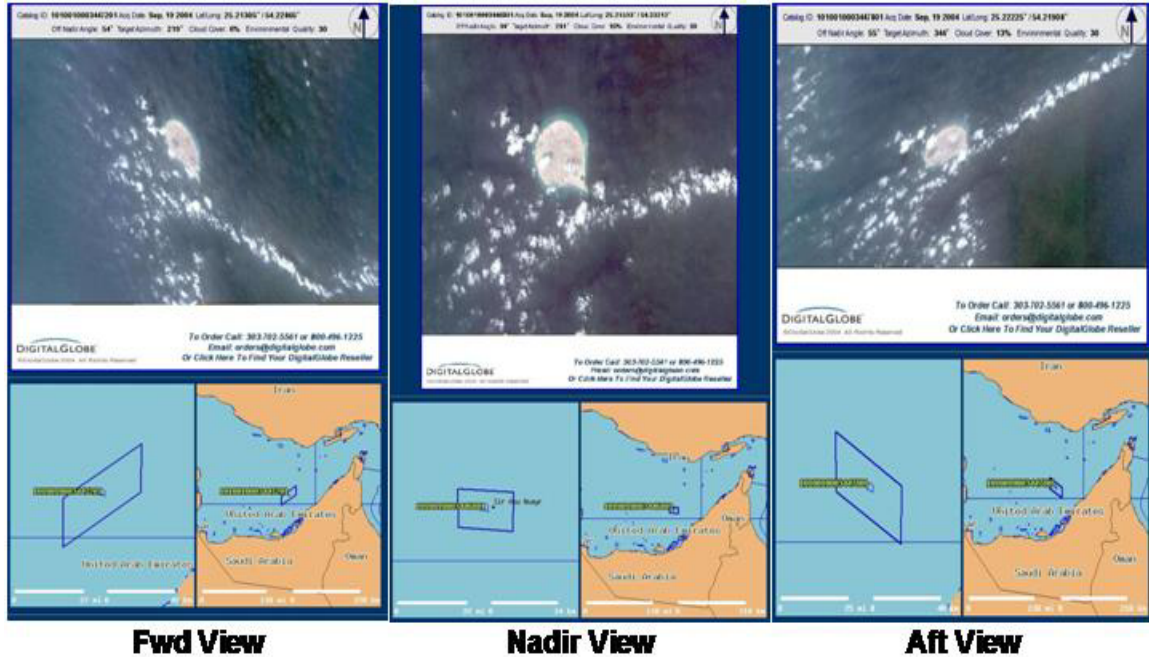


Figure 1. Overview of QB scenes at 60, 37, and 61-degree view angles, respectively (© 2004 DigitalGlobe, Inc. All rights reserved)

The QUICKBIRD-2 data used in this thesis were acquired through National Geospatial-Intelligence Agency (NGA) after being processed and georeferenced by DigitalGlobe ground stations.

Channel	Bandwidth (nm)	Spatial Resolution (m)
1	450 – 520	3.6-7.9
2	520 – 600	3.6-7.9
3	630 – 690	3.6-7.9
4	760 – 900	3.6-7.9

Table 1. QB bandwidth and spatial resolutions (After DigitalGlobe 2004)

2. Multi-angle Imaging SpectroRadiometer (MISR)

The MISR instrument contains nine pushbroom-type telescopes where pixels in cross-track rows are scanned one line at a time as the satellite orbits overhead. MISR is

deployed aboard the National Aeronautics and Space Administration's (NASA) Terra Earth Observing System (EOS) satellite launched in December 1999. Terra is a polar orbiting satellite in a sun-synchronous orbit at an altitude of 705 km with a 98.3-degree inclination and a period of 98.88 minutes. The sun-synchronous orbit allows Terra to pass directly overhead a given location at approximately 1030 local solar time each day and with MISR's 360 km swath, provides for a two to nine day revisit period at the poles and equator, respectively (JPL 2004).

MISR uses nine discrete telescopes pointed at set angles. One telescope views the nadir direction (straight downward beneath the satellite) and four each view the forward and aft directions along the satellite ground track for a total of nine view directions. Thus, in addition to the nadir view, the telescopes view the Earth at 26.1, 45.6, 60.0, and 70.5 degrees forward and aft of the local vertical. The fore and aft telescope angles are the same (i.e. the telescopes are arranged symmetrically about the nadir.) Each telescope uses four Charge-Coupled Device (CCD) line arrays that are filtered to provide one of the four MISR spectral bands. In general, large viewing angles provide enhanced sensitivity to atmospheric aerosol effects and to cloud reflectance effects whereas smaller angles are used for land surface viewing (AOD ATBD 2004). Table 2 provides the telescope angles and spatial resolutions. Table 3 provides the bands primary and secondary uses.

This study uses primarily the 275 m red and NIR channels of the nadir, 45.6, and 60-degree telescopes. Successive images are spaced approximately 1 minute apart, resulting in a total collection time of 5 minutes. The raw MISR data are processed by the Atmospheric Sciences Data Center (ASDC) and then archived and distributed by the Langley Research Center Distributed Active Archive Center (LARC DAAC).

MISR
TYPICAL CAMERA CONFIGURATION

- [Dark Green Box] 275 METERS x 275 METERS (1 x 1)
- [Yellow Box] 1.1 KILOMETER x 1.1 KILOMETER (4 x 4)
- [Blue Box] 275 METERS x 1.1 KILOMETER (1 x 4)

CAMERAS:	Df	Cf	Bf	Af	An	Aa	Ba	Ca	Da
ANGLES:	70.5	60.0	45.6	26.1	0.0	26.1	45.6	60.0	70.5
443 nm									
555 nm									
670 nm									
865 nm									

Table 2. MISR telescope angles and spatial resolutions (From JPL 2004)

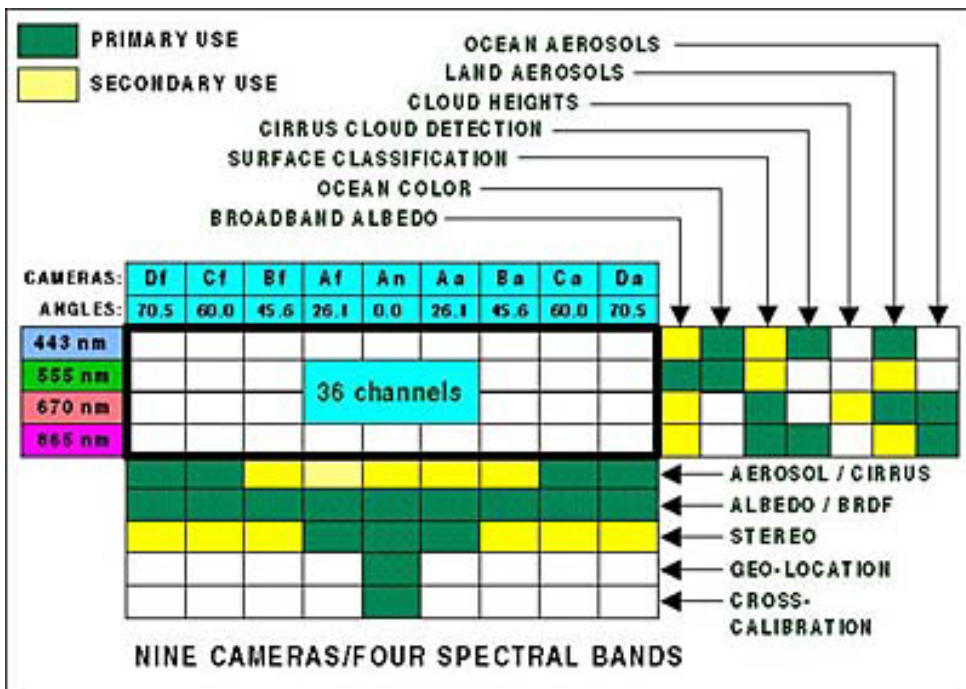


Table 3. MISR bands primary and secondary uses (From JPL 2004)

3. MODerate Resolution Imaging Spectroradiometer (MODIS)

The MODIS instrument is a rotating scan mirror-type imager deployed aboard NASA's Terra Earth Observing System (EOS) satellite, launched December 1999. Terra is a polar orbiting satellite in a sun-synchronous orbit at an altitude of 705 km with a 98.3 degree inclination and a period of 98.88 minutes. The sun-synchronous orbit allows Terra to pass directly overhead a given location at approximately 1030 local solar time each day and with MODIS's 2,330 km swath, provides for global coverage every one to two days and exact orbit repeat every 16 days (ESM Satellites 2004).

MODIS measures radiant and solar-reflected energy from sampled areas of the Earth in 36 spectral bands between 0.405 and 14.385 μm . MODIS has nominal spatial resolutions of 250 m in two bands, 500 m in five bands, and 1000 m in the remaining 29 bands. Table 4 lists the primary use of each band and its maximum spatial resolution. This research paper uses primarily the red and NIR channels (Ch 1 and 2) at 250m resolution. The raw MODIS data were processed by the MODIS Adaptive Processing System (MODAPS), then archived and distributed by the Goddard Space Flight Center (GSFC) Earth Sciences Distributed Active Archive Center (GES DAAC).

Primary Use	Band ¹	Bandwidth (nm)	Spectral Radiance ²	Required SNR ³
Land/Cloud/Aerosols Boundaries	1	620 - 670	21.8	128
	2	841 - 876	24.7	201
Land/Cloud/Aerosols Properties	3	459 - 479	35.3	243
	4	545 - 565	29.0	228

¹ Bands 1 and 2 are 250m spatial resolution; Bands 3 and 4 are 500m spatial resolution
² Spectral Radiance values are ($\text{W}/\text{m}^2 \cdot \mu\text{m} \cdot \text{sr}$)
³ SNR = Signal-to-noise ratio
Note: Performance goal is 30-40% better than required

Table 4. MODIS bands used in study: primary uses, resolutions, and bandwidths (After GSFC 2004)

4. Advanced Very High Resolution Radiometer (AVHRR)

The AVHRR/3 instrument is a flat scanning mirror-type imager deployed aboard the National Oceanic and Atmospheric Administration Polar-orbiting Operational

Environmental Satellites (NOAA POES). The NOAA-17 version used in this study was launched in June 2002. POES is a polar orbiting satellite in a sun-synchronous orbit at an altitude of 811 km with a 98.7-degree inclination and a period of 101.2 minutes. The sun-synchronous orbit allows POES to pass directly overhead a given location at approximately 1030 local solar time each day and, with a 2,894 km swath, provides for global coverage every days with exact orbit repeat every 9 days.

POES uses a 20.3 cm telescope to measure radiant and solar-reflected energy from sampled areas of the Earth in six spectral bands between 0.580 and 12.5 μm . POES has nominal spatial resolutions of 1,090 m. Table 5 lists the spectral characteristics of the AVHRR/3. This thesis uses primarily the red and NIR channels (Ch 1 and 2). The POES data is archived in NOAA's Comprehensive Large Array-data Stewardship System (CLASS) electronic library.

Channel	Bandwidth (nm)	Resolution (m)
1	580 – 680	1090
2	725 – 1000	1090

Table 5. AVHRR bands used in study: spectral and spatial resolution (After NOAA KLM Users Guide 2004)

5. AERosol RObotic NETwork (AERONET)

AERONET is an optical ground based aerosol monitoring network and data archive supported by NASA's EOS and expanded by cooperation with many non-NASA institutions. The network consists of nearly identical automatic sun-sky scanning spectral radiometers owned by various national agencies and universities. Data from this collaboration provides globally distributed near real time observations of aerosol spectral optical depths, aerosol size distributions, and precipitable water in diverse aerosol regimes. The data undergo preliminary processing (real time data), reprocessing (final calibration ~6 mo. after data collection), quality assurance, archiving and distribution from NASA's GSFC master archive and several identical databases maintained globally. The data provides algorithm validation of satellite aerosol retrievals and as well as characterization of aerosol properties that are unavailable from satellite sensors.

The AERONET instrument suites include a CIMEL Electronique 318A spectral radiometer – a solar powered weather hardy robotically pointed sun and sky spectral radiometer with spectral bands at 340, 380, 440, 500, 670, 870, and 1020 nm. Bandwidths are 2 nm for the 340 and 380 nm bands and 10 nm for all other bands. The sensor head is fitted with 25 cm collimators that systematically point the sensor head at the sun according to a preprogrammed routine. See http://aeronet.gsfc.nasa.gov/F_Info/system_info_additional.html for additional information. The data is transmitted from the AERONET site to GSFC for processing. There are three levels of processing; real-time (Level 1.0), cloud screened (Level 1.5), and quality assured (Level 2.0). The Level 1.0 and 1.5 data for this study was acquired from the AERONET GSFC database.

THIS PAGE INTENTIONALLY LEFT BLANK

IV. METHODS AND PROCEDURES

A. AERONET DATA

This study used Level 1.0 real-time data since the Level 1.5 quality-assured data yielded no AOD values due to suspected cloud contamination during satellite overpass times and Level 2.0 quality-assured data is not yet available for this station. However, based on satellite imagery coincident to the AERONET sampling times, no clouds were observed obscuring the AERONET site. Smirnov *et al.* (2000) found that the AERONET cloud screening and quality control algorithm might sometimes incorrectly screen variable aerosol plumes.

The environment around Sir Bu Nuair (SBN) may contain such variable aerosol plumes. Sir Bu Nuair is a 14.3 km² island in the southeastern Arabian Gulf, 70 km from the UAE mainland. The AERONET station senses both terrestrial aerosols from the island as well as marine aerosols from the surrounding water. Sea Surface Temperatures (SST) and land surface temperatures were still very high in September, with an air temperature and SST of approximately 32° and 30° C, respectively. The red wavelength AOD was averaged during the satellite overpass window from 0645Z-0715Z for comparison with the NPS AOD algorithm and MISR AOD algorithm.

B. SATELLITE DATA

Due to the small scan-spot size of QuickBird, sub-scenes were created for the other satellite data to approximately match the geographic coverage area of QuickBird. Figure 2 shows the red wavelength at varying resolutions for AVHRR, MODIS, MISR, and QB. All five images encompass roughly the same geographic area. Scene matching to QB allows for comparison of features and radiances used in the AOD model.

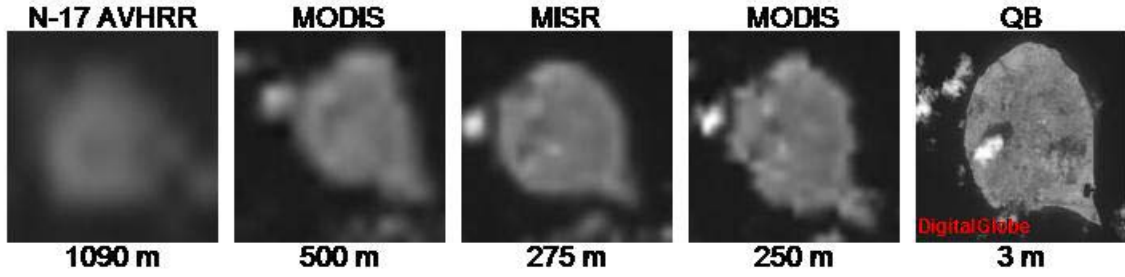


Figure 2. Red wavelength of AVHRR, MODIS, MISR, MODIS and QB at increasing spatial resolutions (© 2004 DigitalGlobe, Inc. All rights reserved)

Given the small scan-spot area of 487 km^2 , this thesis assumed the AOD values recorded by the AERONET station applied to the entire scene. Since the water-dominated scenes had some land and cloud pixels, the scenes were radiometrically smoothed by creating histograms in the red and NIR wavelengths to determine the dominant radiance. Since the scene contained mostly water pixels, the water radiances dominate the distribution of radiances. Figure 3 is a histogram using the full MISR scene in the red and NIR wavelengths showing the multiple radiance peaks associated with land, water, and cloud radiances. Figure 4 is a true color 275 m MISR image of the area for reference. The red wavelength peaks in figure 3 at 164, 125, 33, and 24 $\text{W/m}^2 \mu\text{m sr}$ are indicated in figure 4 as A, B, C, and D, respectively. Similar peaks exist for the NIR wavelength.

The MISR peak at $24 \text{ W/m}^2 \mu\text{m sr}$ corresponds well to the $28 \text{ W/m}^2 \mu\text{m sr}$ radiance QuickBird peak of the water-dominated scene in figure 5. By plotting the number of pixels on a logarithmic scale, figure 5 shows the more subtle peaks associated with the shoal water and the few land and cloud pixels in the scene. The regular dips in the red band are possibly due to an error in the on-board digitization of the raw data.

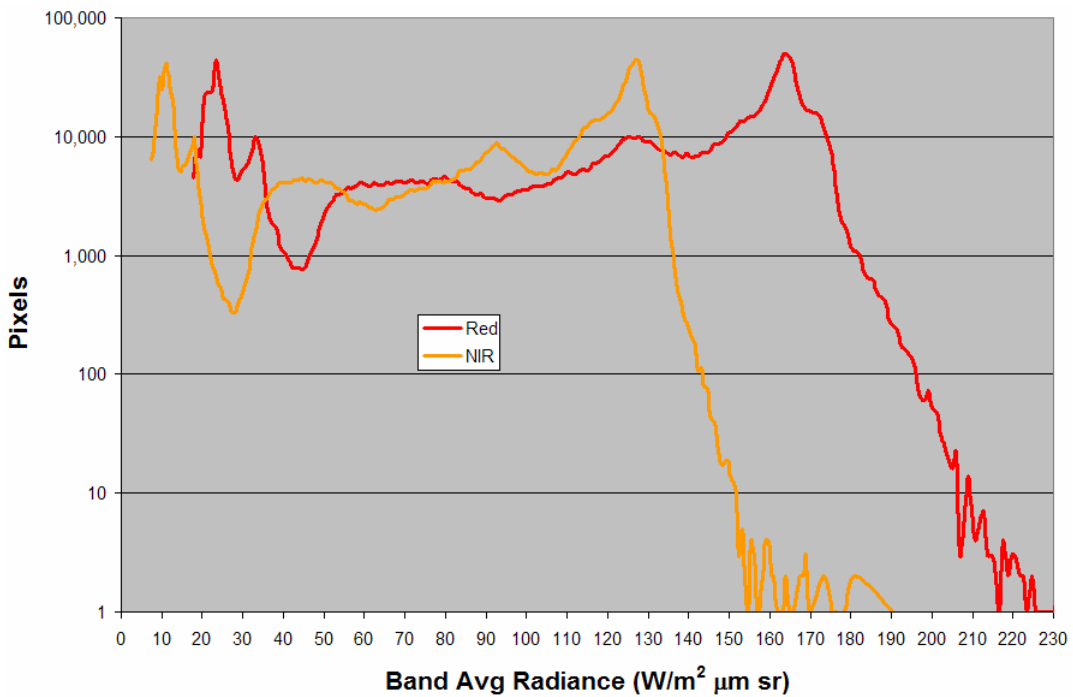


Figure 3. MISR full-scene red and NIR band histograms

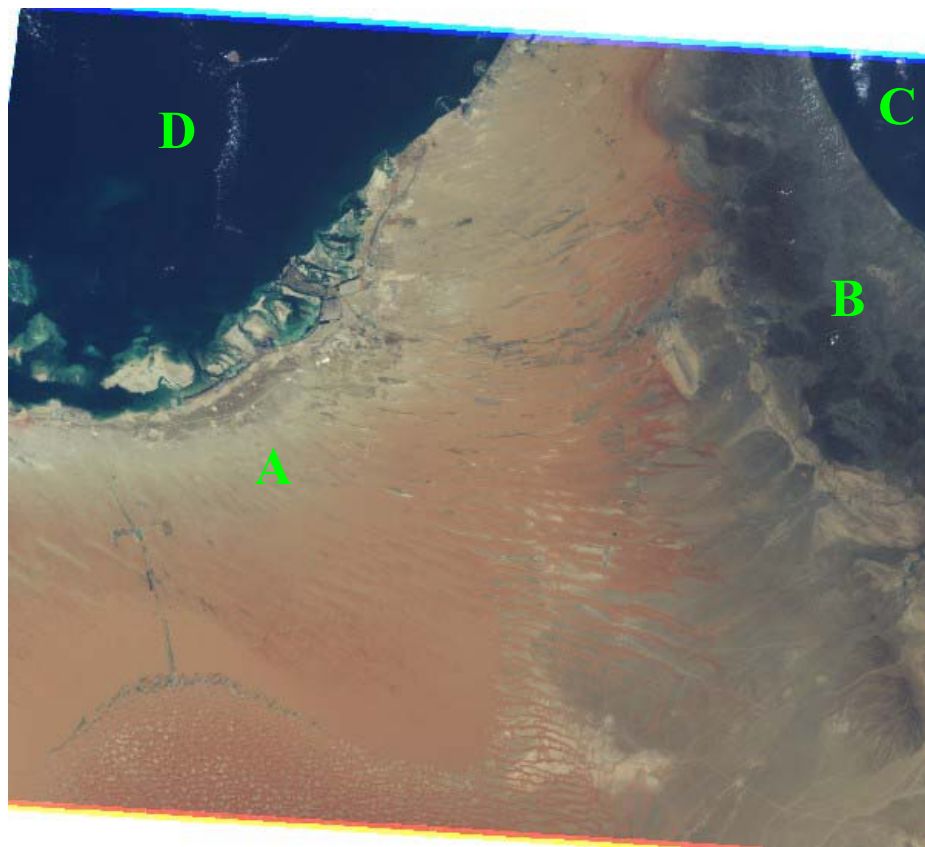


Figure 4. MISR true color image indicating areas of significant red modal radiance peaks

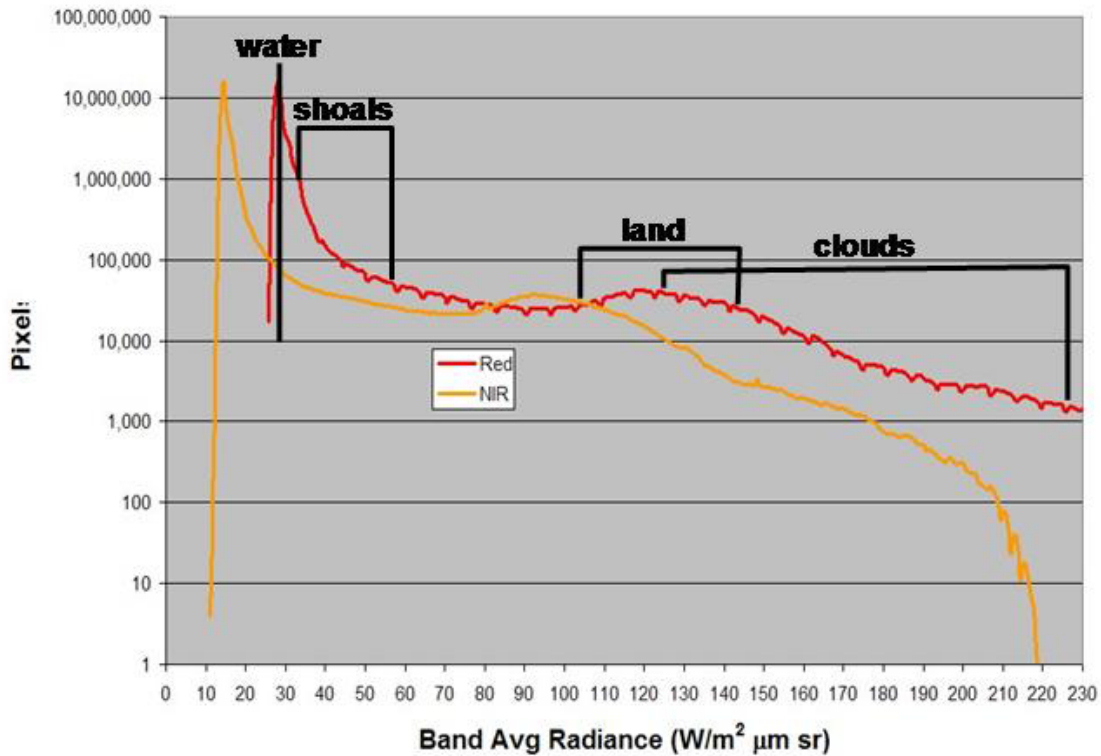


Figure 5. QuickBird nadir view red and NIR band histograms with annotated observed radiances.

The NPS AOD algorithm was originally formulated for NOAA-14 AVHRR. Applying the NPS AOD algorithm to sensors that are sensitive to different wavelengths than the NOAA-14 AVHRR requires that the radiances be adjusted. The modal radiances from the other sensors were linearly extrapolated to match the effective red and NIR wavelengths of NOAA-14 AVHRR. This study assumed a linear extrapolation based on the bandwidths shown on the Wehrli Spectrum in figure 6. Linear extrapolation is a valid approach since E_0 is linear and scattering mechanisms are nearly linear at these wavelengths. The extrapolated modal radiances were used in the NPS AOD algorithm as the input top of the atmosphere radiance (L_t).

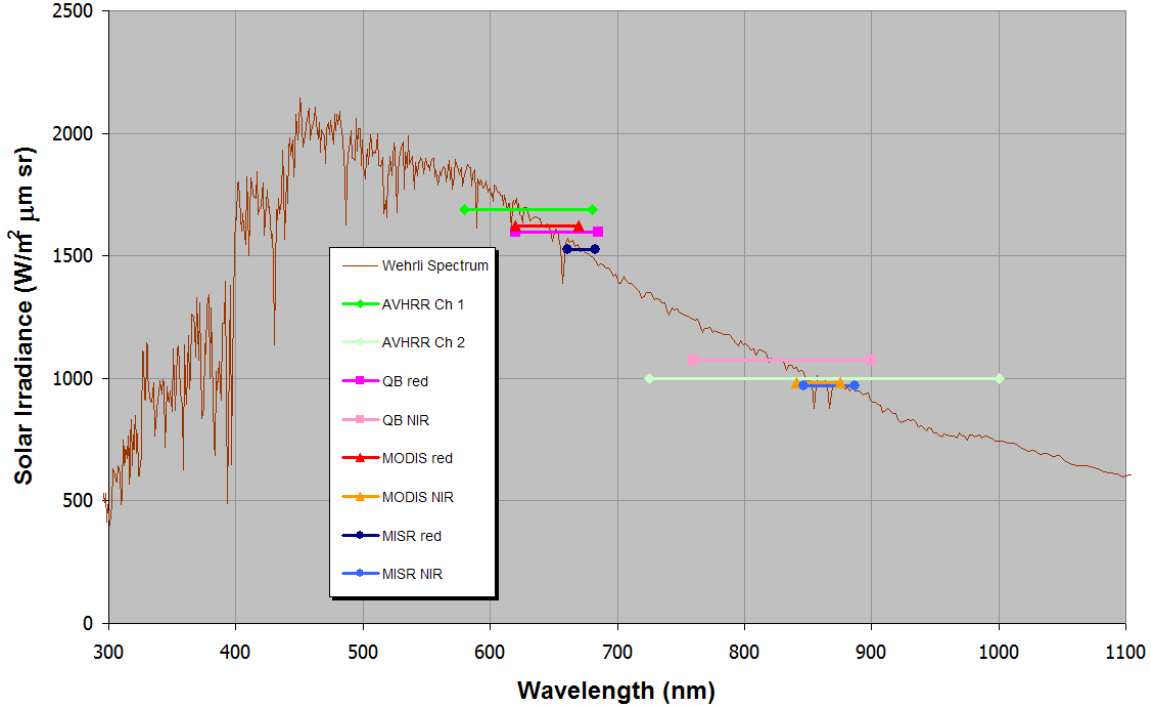


Figure 6. Wehrli solar irradiance spectrum with applicable satellite bandwidths.

Lastly, it appears the QuickBird radiances calibrate too high for a given scattering angle. This theory is based on a comparison with MODIS, whose red band characteristics and scattering angle for this case are closest to QuickBird. Figure 7 shows the red modal radiances plotted against scattering angle. Note that while the QuickBird nadir and MODIS 250 m data have nearly the same scattering angle, the QuickBird radiance is $1.62 \text{ W/m}^2 \mu\text{m sr}$ or 6.2% higher. In addition, since the E_0 for MODIS is $22 \text{ W/m}^2 \mu\text{m sr}$ or 1.4% higher than QuickBird, essentially, QuickBird radiance is approximately 7.6% too high for this single instance. Multiple cases of sensor comparisons are necessary to draw firm conclusions regarding relative calibration accuracy.

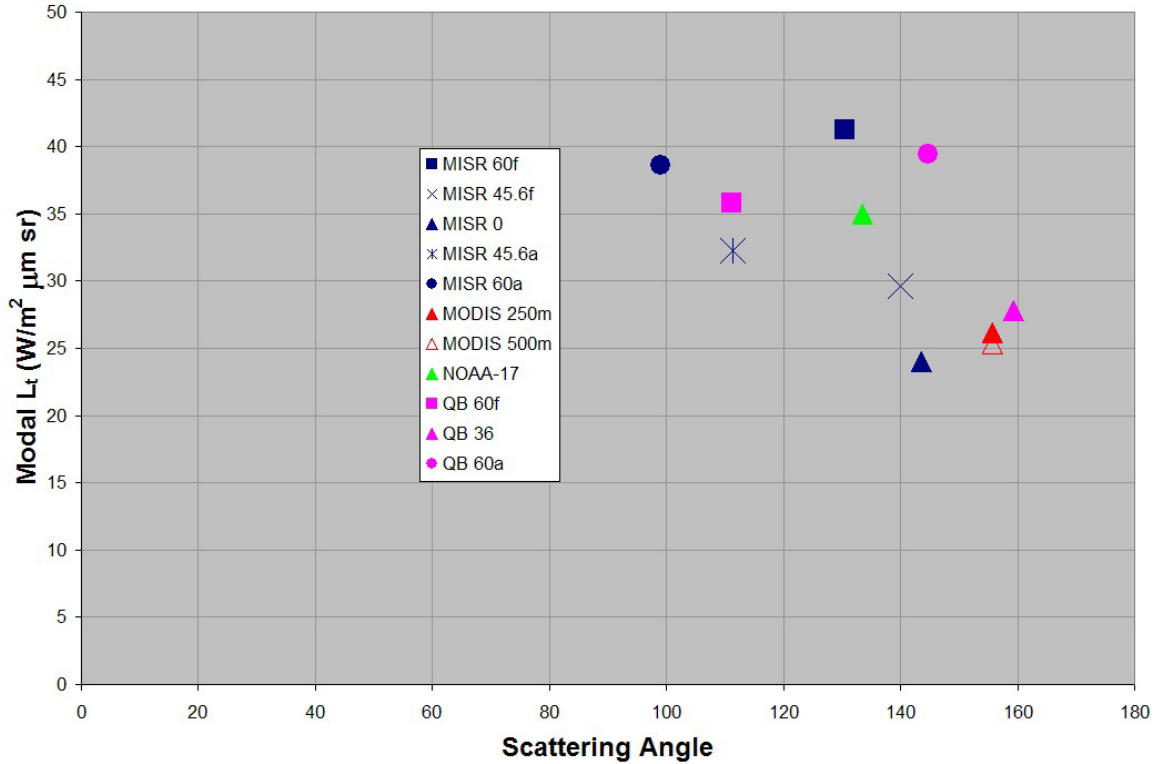


Figure 7. Red modal top of the atmosphere radiance (L_t) vs. scattering angle

C. AOD ALGORITHMS

1. NPS

This algorithm applies linearized, single-scatter theory with an estimate of bidirectional surface reflectance. Using a technique developed by Durkee *et al.* (1991), scattering phase functions are parameterized to seven aerosol model size distributions typically found in a marine environment as developed by Brown (1997). A particle size parameter (S12) is calculated using the ratio of the red and NIR wavelength L_α 's. The S12 value and scattering angle are used to determine an aerosol model index (AMI). Mie theory is used to calculate scattering phase function curves for each aerosol model size distribution. The AMI and the scattering angle determine the scattering phase function that is needed to calculate aerosol optical depth.

The NPS AOD model provides AOD estimates in this thesis according to Brown (1997) and Smith (1998) with the following exceptions. Instead of inputting radiances for individual pixels, a linearly extrapolated modal radiance was inputted as described in Section IV, B above. In-band Solar Irradiance (E_0) was calculated for each satellite based

on the Wehrli (1985) Solar Irradiance Spectrum shown in figure 6. Due to narrower bandwidths, the QuickBird, MISR, and MODIS avoid a peak ozone absorption band at approximately 599 nm, hence the ozone correction was halved compared to the AVHRR correction. Figure 8 illustrates the transmittance as a function of wavelength with the satellite bandwidths plotted for reference.

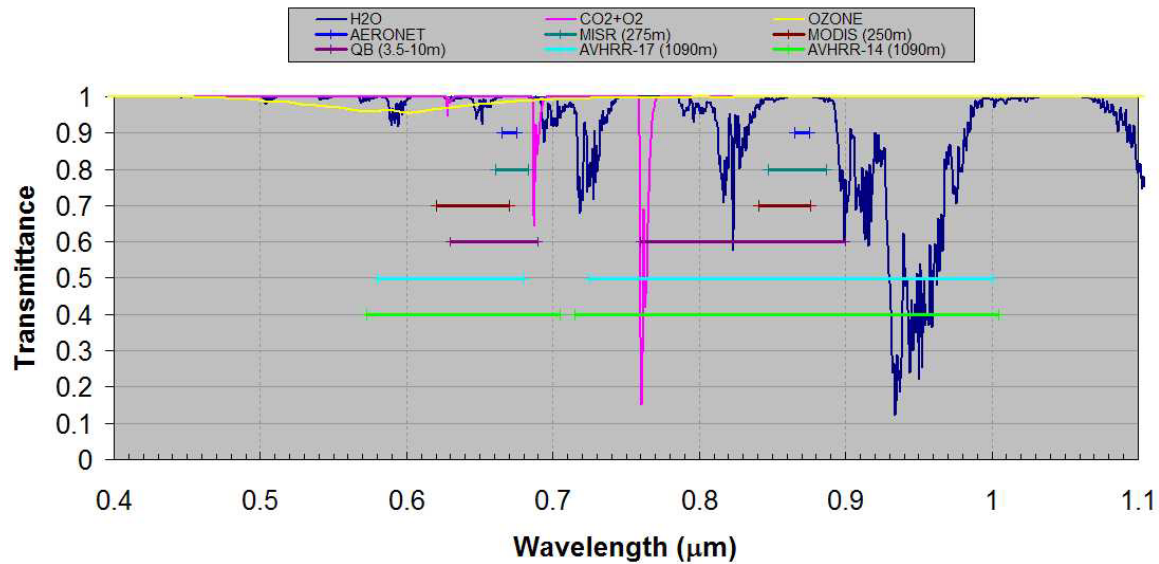


Figure 8. Transmittance as a function of wavelength with applicable sensor bandwidths and atmospheric absorption gases.

Figure 9 shows the partial results of a study by Smith (1998) using ACE-2 data to validate the NPS AOD model. For that study, the model performed well, especially at low AOD's as shown in figure 9. Smith (1998) theorized that the degradation in model performance at higher AOD's was in part due to the non-absorbing assumption the model uses even in dust aerosol environments where the single scatter albedo may actually be less than one.

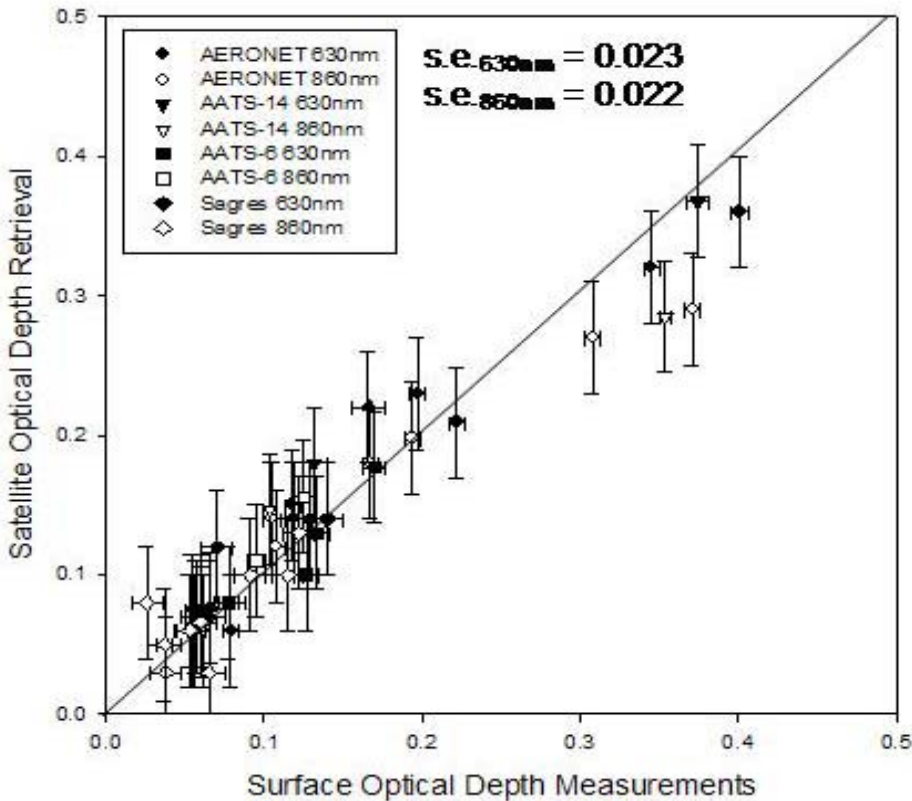


Figure 9. Scatter plot with satellite derived AOD's and surface based AOD's (From Smith 1998)

2. MISR

JPL developed a three-stage AOD algorithm process for the MISR instrument that consists of three sub-algorithms: Dark Water, Dense Dark Vegetation (DDV), and Heterogeneous Land. See MISR ATBD (2001) for full details of the algorithm summarized below.

Stage 1 – Once an area is determined to be valid using other MISR products and datasets, the area's spatial resolution is sub-sampled to 17.6 km and the radiances are calibrated and converted to reflectances. An ozone absorption correction is applied and contaminated subregions or channels are filtered out.

Stage 2 – If the pixel is over the water, based on a geographic location database, the Dark Water Flag is set. If the pixel is not over the water, the corrected reflectances are searched for Dark Dense Vegetated (DDV) regions. If DDV regions are found, the DDV flag is set. If no DDV regions are found, Empirical Orthogonal Functions (EOF)

are calculated and if sufficient contrast exists, the Heterogeneous Land Flag is set. If none of the three areas above are found, the algorithm exits.

Stage 3 – The data above and other external datasets are used to calculate the AOD and uncertainty. A final process calculates the Best Estimate AOD that was used in this research paper.

3. NPS vs. MISR

This study provided an opportunity to compare the NPS and MISR AOD algorithms. The MISR AOD algorithm is used in this thesis to validate the use of multi-angle QB views in the NPS AOD model. While the NPS AOD algorithm uses a single view angle and the red and NIR wavelengths, MISR AOD utilizes up to nine view angles and four wavelengths. MISR's use of varying view angles minimizes sun glint, so AOD retrievals occur over regions where a single view angle is contaminated by sun glint. Multiple wavelengths used by MISR allow for AOD retrievals not only over water, but also over certain types of land. The MISR Dark Water algorithm is most similar to the NPS algorithm with respect to wavelength where the red and NIR bands take advantage of the absorbing properties of deep water to create a radiatively dark surface. The DDV algorithm uses the blue and red bands with up to nine view angles for AOD retrievals. Since the Heterogeneous Land algorithm uses EOF's, the wavelengths and view angles are variable.

THIS PAGE INTENTIONALLY LEFT BLANK

V. RESULTS

A. SYNOPTIC WEATHER SITUATION

At 0600Z 19 September 2004, a weak 500 mb ridge extended over the Arabian Gulf and the 500 mb wind was northerly at 5-15 knots. At 850 mb, a thermal low was over the Saudi Arabian Peninsula resulting in southerly flow over the eastern Arabian Gulf. Surface observations near SBN showed a Mean Sea Level Pressure (MSLP) of 1008 mb with easterly winds at 10-15 kts. Surface temperature was 32° C and a dew point of 28° C resulting in a relative humidity of approximately 80%. Sea surface temperatures (SST) around SBN were about 30° C.

High SST and air temperatures create conditions that can cause condensational growth of the aerosol particles with the highest humidity's near clouds. Figure 10 shows a true color nadir QB view of SBN on the left and on the right is the same image with a histogram equalization enhancement applied, heightening the contrast and brightness. The right image shows condensational growth in the immediate vicinity of the scattered clouds around SBN. However, a more interesting feature is located away from the clouds, in the upper and lower right of the right-side image. The aerosol scattering, in conjunction with the high spatial resolution of QB, highlights what appear to be convective parcels within the aerosol. This process is likely due to a combination of the high SST's providing lift from below and the condensational effect making the aerosols large enough to be seen by QB.

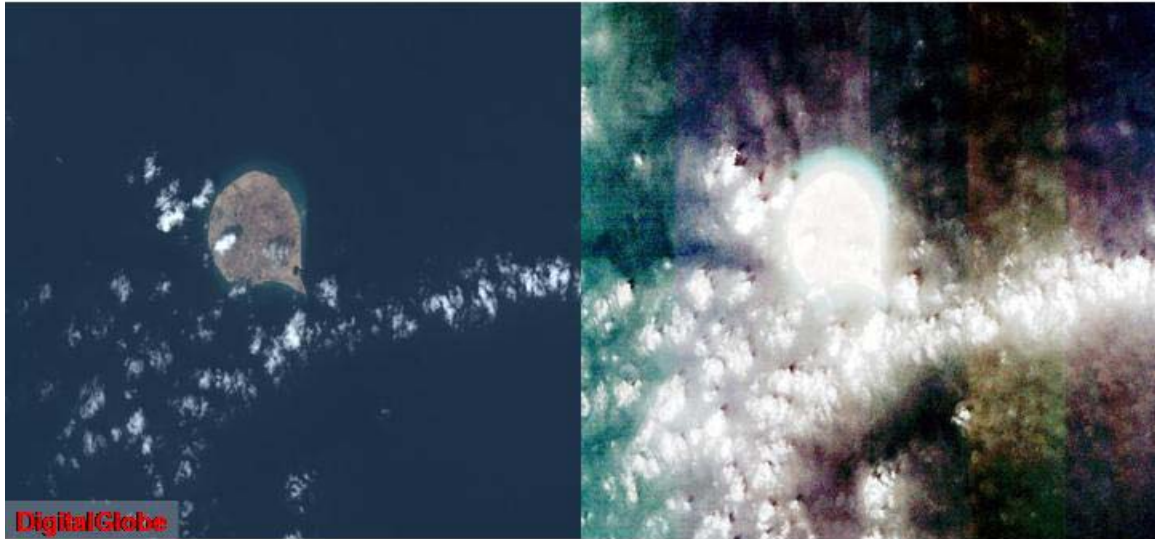


Figure 10. Left image of SBN is a true color nadir QuickBird view; Right image of SBN applies a histogram equalization enhancement to the left image (© 2004 DigitalGlobe, Inc. All rights reserved).

Cloud top temperatures in the scene were very warm at 26-28⁰ C. Figure 11 shows a rawinsonde sounding at Abu Dhabi (~87 km southeast of SBN) with a low level inversion around 925 mb or 700 m. Thus, the aerosols observed at SBN were likely capped at 700 m. With southerly and easterly low-level winds, their source region was likely the UAE desert.

41217 OMAA Abu Dhabi Inter Arpt

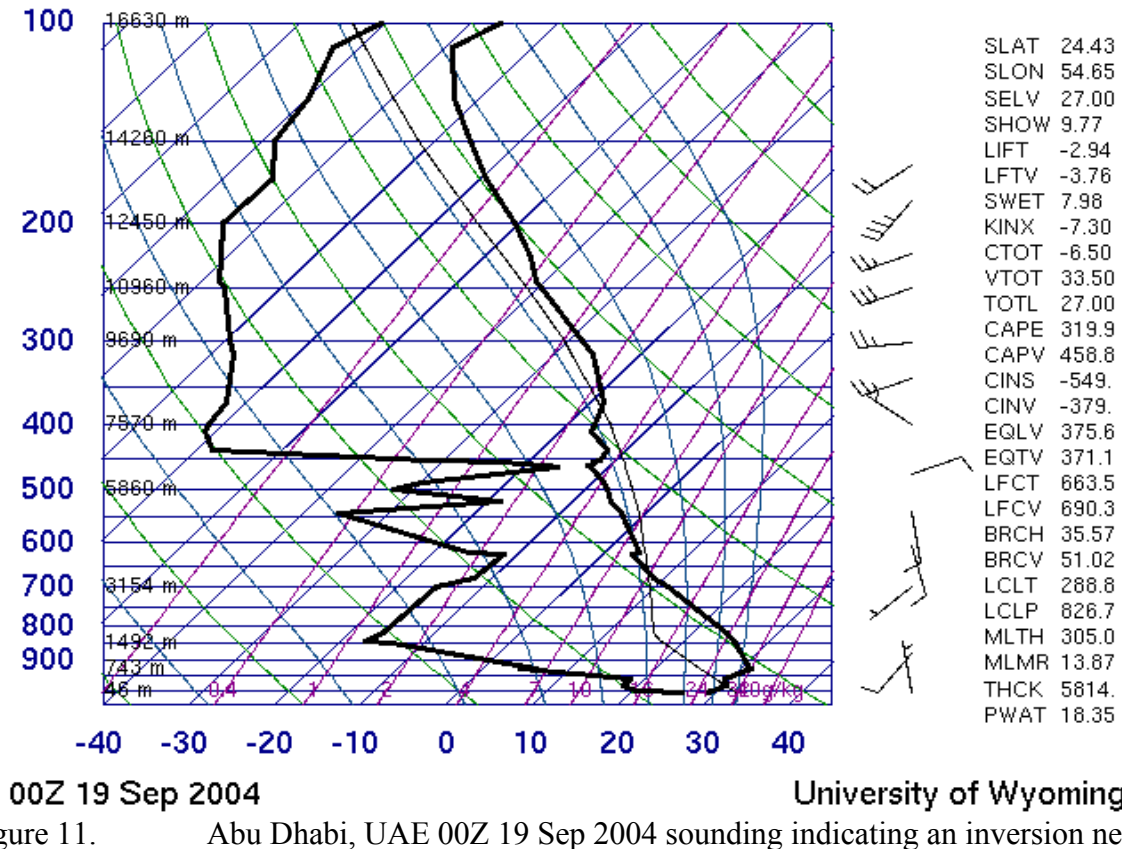


Figure 11. Abu Dhabi, UAE 00Z 19 Sep 2004 sounding indicating an inversion near 925 mb or 700 m (From University of Wyoming 2004).

B. AOD COMPARISONS

Table 6 shows the results of the NPS AOD model for each view, AERONET estimated AOD, and the MISR AOD. The nadir views and MISR AOD all fall within 11% of AERONET indicating good agreement. The high zenith angle AOD's are much too large, possibly due to the increased path length at high zenith angles. The AOD model assumes that most of the radiance measured by the satellite is due to linear single scattering. An increased path length results in a greater chance for multiple scattering to occur and affect L_a . Furthermore, this single study does not allow for good characterization of QuickBird calibration. Francis (personal communication) indicated that DigitalGlobe has not done much quantitative calibration on QuickBird. Therefore, if the top of the atmosphere radiance values entered into the AOD model are inaccurate, the

output will be inaccurate as well. In summary, the assumptions magnify the errors in the AOD model at high zenith angles resulting in high AOD values.

Sensor	Scattering Angle	View Angle	S12 Ratio	aod63	aod86	Angstrom Exponent
MISR 60 deg Fwd	130.41	60.37	1.40	1.06	1.04	0.08
MISR 45.6 deg Fwd	139.92	46.24	1.36	0.78	0.78	0.00
MISR 8 deg Nadir	143.61	8.22	1.38	0.39	0.43	-0.40
MISR 45.6 deg Aft	111.29	45.77	1.58	0.58	0.57	0.07
MISR 60 deg Aft	99.00	60.13	1.57	0.50	0.48	0.17
MODIS 250 m	155.72	9.41	1.51	0.39	0.36	0.33
NOAA-17	133.45	34.29	1.61	0.45	0.35	1.04
QB 60 deg Fwd	111.24	59.90	1.67	0.68	0.59	0.59
QB 36 deg Nadir	159.39	36.90	1.60	0.39	0.33	0.69
QB 60 deg Aft	144.67	61.20	1.58	0.57	0.49	0.63
AERONET at SBN	n/a	n/a	n/a	0.41	0.37	1.05
MISR AOD	n/a	n/a	n/a	0.46	n/a	n/a

Table 6. Scattering angle, view angle, S12 ratio, aod63, aod86, 660-840 Angstrom Exponent sorted by sensor. Green shaded blocks are within 11% of SBN (shaded blue). The SBN estimated Angstrom Exponent is at 500-870 nm.

Figure 12 is the AERONET AOD from approximately 0500-0900Z on September 19, 2004 at varying wavelengths. During the satellite overpass times (0653-0718Z), there is a general increasing trend in AOD. Table 6 shows this increasing trend, as AOD values at nadir views are higher for NOAA-17 AVHRR than for QuickBird. It is also worth noting that most of the calculated Angstrom Exponents are significantly lower than SBN estimated values, possibly due to the logarithmic nature of the exponent, such that small variations in AOD lead to large changes in the exponent. Furthermore, in the cases of multi-angle views, the exponent trend is different for QB and MISR. For MISR, the extreme view angles produce slightly better results than nadir views while for QB the opposite is true.

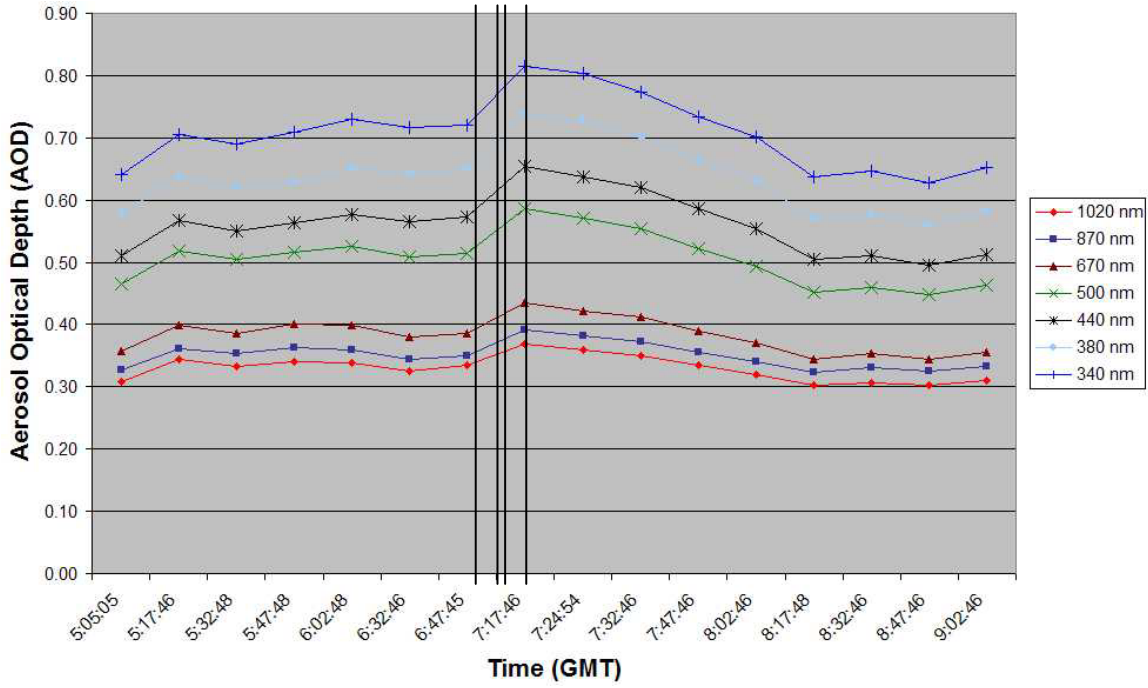


Figure 12. AERONET estimated AOD values at seven wavelengths from 0500-0900Z. Vertical lines, from left to right, indicate satellite overpass times for QB, MODIS, MISR, and AVHRR, respectively.

Figure 13 displays the relation between AOD and zenith angle. AERONET and the MISR AOD do not have zenith angles *per se*, so the dashed line represents the MISR AOD value and the box indicates the range of AERONET AOD estimations. This figure indicates good agreement of nadir QuickBird views and nadir views from other satellites with AERONET estimated AOD. It also shows that at high zenith angles, the AOD values are too large for the reasons discussed above.

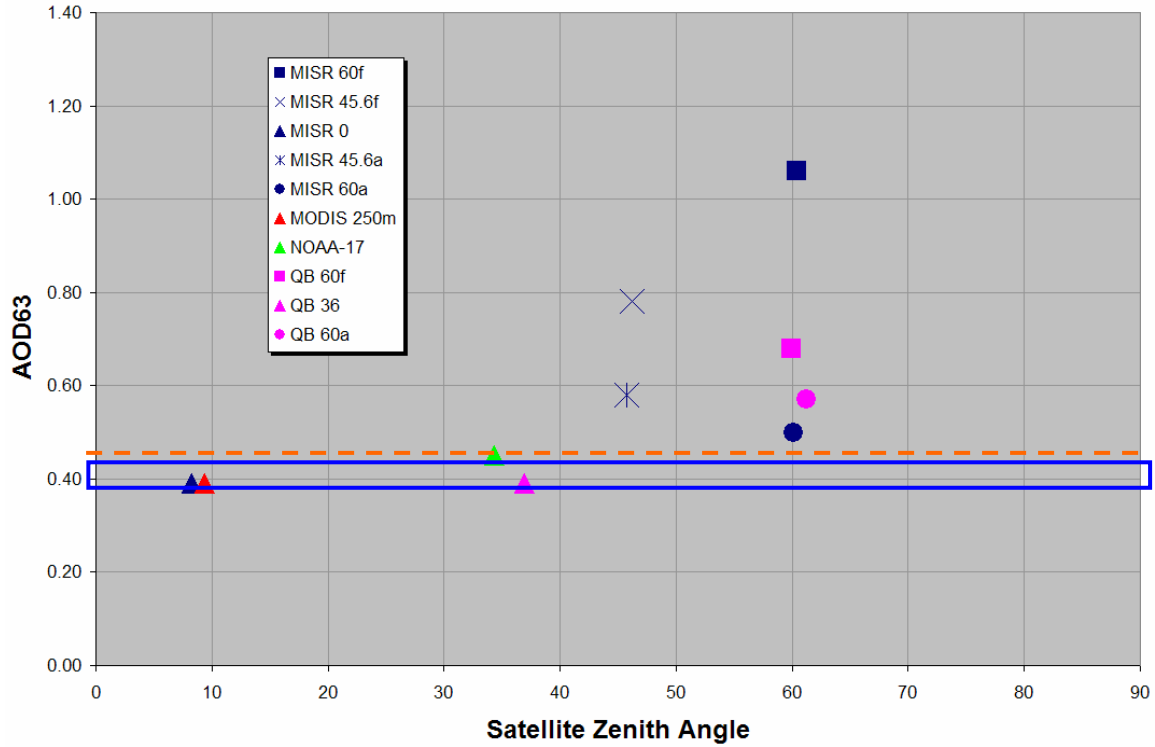


Figure 13. NPS AOD63 (red band) calculated values versus satellite zenith angle. The dashed line indicates the MISR AOD value and the box shows the SBN AERONET estimated AOD range.

Figure 14 shows the relation between the S12 ratio and scattering angle for sensor view angle with the curves for the model aerosol size distributions from Brown (1997). While the S12 ratio values are low for all satellites, a general trend appears in the data. It appears that the QuickBird and AVHRR values demarcate a new curve. This trend appears in the MISR and MODIS data as well, indicating for the Arabian Gulf region, the aerosols are larger than Brown's (1997) curves allow for. The low S12 values indicate a large aerosol size expected in the Arabian Gulf region due to the proximity of numerous desert areas. In addition, within those desert regions are areas of various sands, silts, and clays. Figure 15 shows the AERONET estimated Angstrom Exponent corresponding with the AOD estimate in figure 12. The S12 ratio values in table 6 are consistent with the low 500-870 Angstrom Exponent estimated by AERONET shown in figure 15, in that a low Angstrom Exponent indicates a larger diameter aerosol.

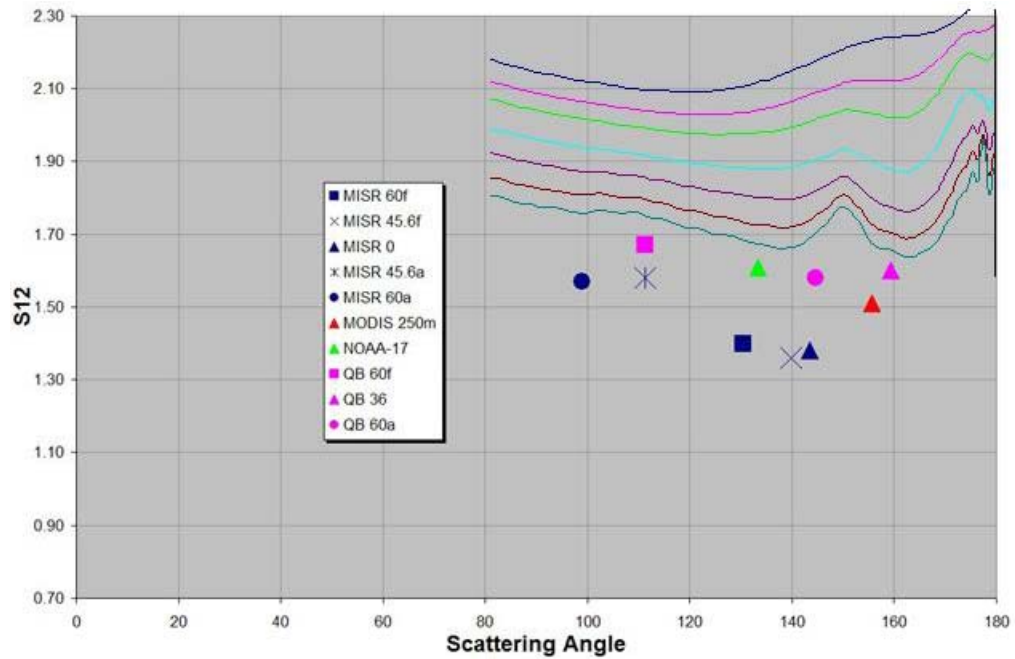


Figure 14. S12 Size Index versus Satellite Scattering Angle with Brown (1997) Aerosol Model Size Distributions

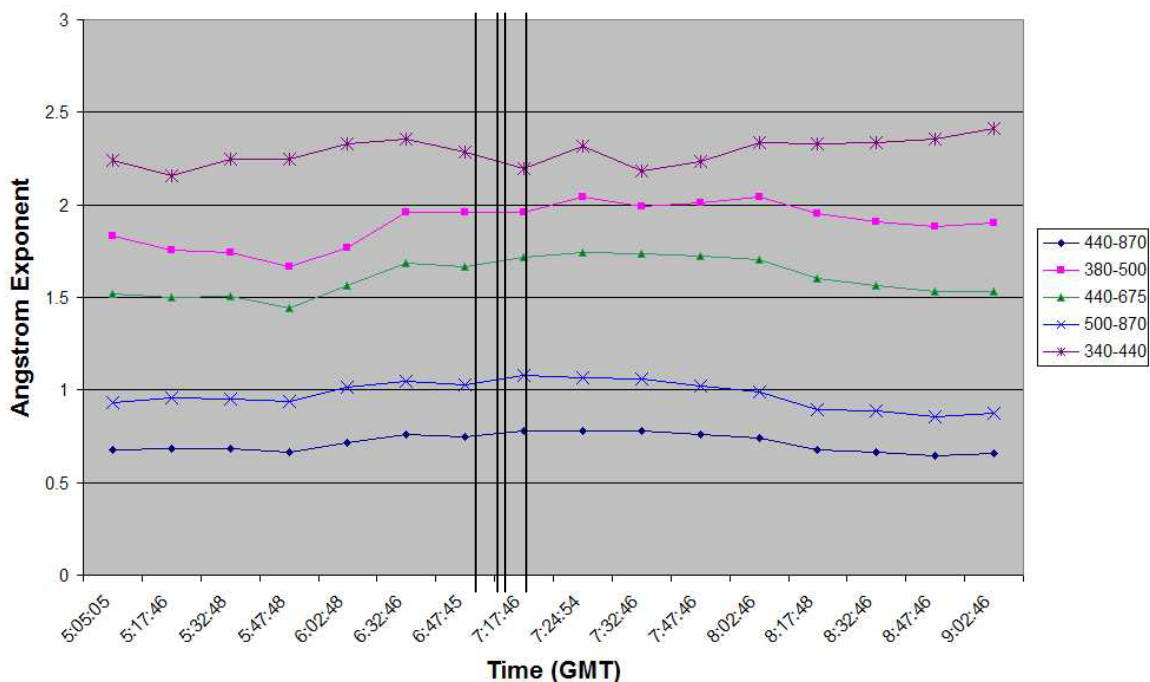


Figure 15. Angstrom Exponent estimated by AERONET between 0500-0900Z

THIS PAGE INTENTIONALLY LEFT BLANK

VI. CONCLUSIONS AND RECOMMENDATIONS

A. CONCLUSIONS

This thesis assesses using very high spatial resolution QuickBird satellite data with the NPS AOD algorithm. Data from multiple satellites with overpass times within 30 minutes of each other was collected around Sir Bu Nuair Island off the western coast of UAE on September 19, 2004. An AERONET station on SBN estimated *in situ* AOD's. After determining the QuickBird modal radiance for an area approximating the nadir QuickBird scene and linearly extrapolating the modal radiances to NOAA-14 AVHRR effective wavelengths, the NPS AOD model used these modal extrapolated radiances to estimate AOD's. MISR, MODIS, and AVHRR radiances underwent the same procedure before ingestion into the NPS AOD model for comparison with the QuickBird results. The MISR AOD algorithm was compared to the AERONET AOD and NPS AOD results for validation.

Results show application of the NPS AOD model to QuickBird data yields findings that are consistent with other satellite and ground based retrievals. In general, the NPS AOD model works well for nadir and near-nadir view angles, but not for high zenith angles. The weakness of the NPS AOD model at high zenith angles is possibly due to the magnification of errors created by the model assumption of linear single scattering. QuickBird imagery is of sufficient resolution to see detailed structure in the aerosol. This study observed convective parcels in the aerosol outside of cloud regions as well as detailed condensational aerosol growth near clouds.

The S12 ratios are low indicating large aerosols. SBN estimated Angstrom exponents are also low further supporting an environment around SBN consisting of large aerosols. Given low-level wind from the south and east, the source region for large aerosols is likely the deserts in UAE. However, calculated Angstrom Exponents are very low, other than NOAA-17 AVHRR that is very close to SBN estimated values. The low values are most likely due to small errors in the AOD that due to the logarithmic nature of the exponent, result in large errors exponent values.

B. RECOMMENDATIONS

Based on this initial study, the following recommendations are suggested:

- Given the limitations of L_r calculations at high satellite zenith angles, investigate a new L_r algorithm that will correctly deal with high zenith angles. This investigation may be a whole thesis in and of itself.
- QuickBird calibration is not well characterized and needs further investigation. Verify QB calibration by finding cases where the QB geometry is very close to MODIS to allow for direct red wavelength comparisons.
- Conduct similar studies in other marine regions to determine if the techniques investigated in this research paper apply elsewhere. Other possible areas of study include the Yellow Sea, eastern Mediterranean, Red Sea, and eastern Atlantic off the coast of West Africa. These marine regions have a high potential for dust aerosols, similar to the Arabian Gulf
- Develop an additional one or two aerosol size distribution models for large particles. Use of Brown's (1997) methodology by increasing the standard deviation of the new model aerosols distributions to 2.8 and 2.9 would be a valid approach. Kuciauskas (2002) found use of a flatter curve at high scattering angles might be better for non-spherical dust aerosols. The best and most difficult way to develop the new size distributions would be *in situ* measurements from the region of study.

LIST OF REFERENCES

Brown, B. B., 1997: Remote measurement of aerosol optical properties using the NOAA POES AVHRR and GOES Imager during TARFOX. M.S. Thesis, Department of Meteorology, Naval Postgraduate School, Monterey, CA, 73 pp.

Charlson, R. J., S. E. Swartz, J. M. Hales, R. D. Cess, J. A. Coakley, Jr., J. E. Hansen and D. J. Hoffman, 1992: Climate forcing by anthropogenic aerosols. *Science*, **255**, 423-430.

DigitalGlobe, cited 2004: QuickBird specifications. [Available online at <http://www.digitalglobe.com/about/quickbird.html>.]

Durkee, P. A., D. R. Jensen, E. E. Hindman, and T. H. Vonder Haar, 1986: The relationship between marine aerosol particles and satellite-derived radiance. *J. Geophys. Res.*, **91**, 4063-4072.

_____, F. Pfeil, E. Frost, R. Shema, 1991: Global analysis of aerosol particle characteristics. *Atmos. Environ.*, **25(A)**, 2457-2471.

Francis, Lynn, 2004: Email from DigitalGlobe Customer Service Technical Support Manager received on 23 November 2004 [lfrancis@digitalglobe.com].

Goddard Space Flight Center, cited 2004: MISR Level 2 Aerosol Retrieval Algorithm Theoretical Basis. [Available online at http://eospso.gsfc.nasa.gov/eos_homepage/for_scientists/atbd/docs/MISR/atbd-misr-09.pdf.]

Goddard Space Flight Center, cited 2004: MODIS Technical specifications. [Available online at <http://modis.gsfc.nasa.gov/about/specs.html>.]

Intergovernmental Panel on Climate Change. *Climate Change 2001 – The Scientific Basis* (contribution of working group I to the Third Assessment Report of the Intergovernmental Panel on Climate Change). Cambridge University Press, Cambridge, 2001.

Kiehl, J. T. and B. P. Briegleb, 1993: The relative roles of sulfate aerosols and greenhouse gases in climate forcing. *Science*, **260**, 311-314.

Jet Propulsion Laboratory, cited 2004: MISR Instrument. [Available online at <http://www-misr.jpl.nasa.gov/mission/minst.html>.]

Kuciauskas, A. P., 2002: Aerosol optical depth with NOAA GOES and POES in the Western Atlantic. M.S. Thesis, Department of Meteorology, Naval Postgraduate School, Monterey, CA, 83 pp.

Liou, K. N., 1980: *An Introduction to Atmospheric Radiation*. Academic Press, New York, 392 pp.

National Aeronautics and Space Administration cited 2004: Earth Science Mission Terra. [Available online at http://gaia.hq.nasa.gov/ese_missions/satellite_52.htm.]

National Oceanographic and Atmospheric Administration cited 2004: NOAA KLM User's Guide Section 3.1 [Available online at <http://www2.ncdc.noaa.gov/docs/klm/html/c3/sec3-1.htm>.]

Naval Research Laboratory-Monterey cited 2004: UAE² Science Plan [Available online at http://www.nrlmry.navy.mil/aerosol/Case_studies/uae2/exec_summary.html.]

Smith, P. J., 1998: Remote measurement of aerosol optical properties using the NOAA POES AVHRR during ACE-1, TARFOX, and ACE-2. M.S. Thesis, Department of Meteorology, Naval Postgraduate School, Monterey, CA, 59 pp.

Turner, R., 1973: Atmospheric effects in remote sensing. *Remote Sensing of the Earth Resources, II*, F. Shahrocki, Ed., University of Tennessee, 549-583.

Twomey, S. A., M. Piepgrass, and T. L. Wolfe, 1984: An assessment of the impact of pollution on the global albedo. *Tellus* **36B**, 356-366.

University of Wyoming cited 2004: Atmospheric Soundings [Available online at <http://weather.uwyo.edu/upperair/sounding.html>.]

INITIAL DISTRIBUTION LIST

1. Defense Technical Information Center
Ft. Belvoir, Virginia
2. Dudley Knox Library
Naval Postgraduate School
Monterey, California
3. Chairman, Code MR
Department of Meteorology
Naval Postgraduate School
Monterey, California
4. Professor Philip A. Durkee (Code MR/DE)
Department of Meteorology
Naval Postgraduate School
Monterey, California
5. LCDR Joseph S. Martin
Naval Postgraduate School
Monterey, California